https://doi.org/10.1016/j.compositesb.2020.108600

Thermal stability and high-temperature mechanical performance of naostructured W-Cu-Cr-ZrC composite

Lijun Gao [a], Chao Hou[a], Fawer Tang[a], Shuhua Liang[b], Junhua Luan[c],Zengbao Jiao[d], Chao Liu[e,]

[a] *Faculty of Materials and Manufacturing, Key Laboratory of Advanced Functional Materials, Ministry of Education of China, Beijing University of Technology, Beijing 100124, China*

[b] *Xiamen Tungsten Co., Ltd., Xiamen 361009, China*

[c] *Department of Materials Science and Engineering, City University of Hong Kong, Hong Kong, China*

[d] *Department of Mechanical Engineering, The Hong Kong Polytechnic University, Hong Kong, China*

[e] *State Key Laboratory of Powder Metallurgy, Central South University, Changsha 410083, China*

Abstract

Improvement of high-temperature mechanical properties of W–Cu based composites is highly desirable but still a challenge. Here it is achieved by combined effects of solid solution, dispersed nano-precipitation and highly stabilized nanostructure in the W–Cu–Cr–ZrC composite, which takes advantage of the in-situ precipitated Zr–Cr–C nanoparticles and phase-separated Cr thin films. The grain size of W phase in the W–Cu–Cr–ZrC composite retained at the nanoscale up to 1000℃ (close to Cu melting point) for a long duration. The high thermal stability of the nanostructure endows the composite with a compressive strength of 1150MPa at 900 ℃, which is approximately four times as high as that of the binary coarse-grained W–Cu composite. The effects of

microstructure evolution on the mechanical properties at high temperatures and its mechanisms were disclosed. The results indicated the crucial role of the microstructural stability of W phase skeleton in the overall strength of the W–Cu based composites

Keywords: W–Cu based Composite Nanostructure Thermal stability Strength

1. Introduction

W–Cu based composites have been widely used in high-temperature applications, such as nozzle throat lining of rocket and gas rudder of missile[1–4]. As proposed, the metal matrix composites for high-temperature applications need to be constructed using sufficiently strong refractory matrix[5]. When served at elevated temperatures, the W skeleton is used to support the composite, as the Cu phase may become soft or even vaporize[6–9]. Therefore, the structural stability of the W phase at high temperatures is very important to the mechanical performance hence the service reliability of the W–Cu based compo- nents[10–12].

Up to now, the strategies to strengthen the W–Cu composites have been mainly focused on the grain refinement and addition of dispersive nanoparticles. Oxides[13–16] or refractory carbides[17–20] with higher melting points were introduced to inhibit the migration of grain boundaries, or to improve the bonding strength between the immiscible W and Cu phases. In addition, some researchers designed compositionally gradient[21] or hierarchical[22] structures to reduce the interfacial thermal stress caused by the mismatch of thermal expansion coefficients between W and Cu, and thus the mechanical properties of the composites were improved[23–26]. However, the grain size of W in those

composites obtained by the above methods are mostly in the micron-scale, generally larger than 200nm. Thus the increase in the mechanical properties of the composites is limited, e.g. the hardness of

the coarse-grained W–Cu composites reported in the literature ranges from 230 HV to 409 HV[27–29]. If the structure is further refined to the nanoscale, it is expected that the mechanical performance of the W–Cu composites will be greatly improved[30].

In order to prepare the nanostructured W–Cu based composites, we developed an in-situ method in our previous work for synthesizing the W–Cu nanopowders with highly dispersive refractory carbide nanoparticles[31]. The W–Cu nanopowders were subsequently densified by the spark plasma sintering (SPS) technique. The resultant W–Cu composite bulk had hierarchical structure with nanocrystalline microstructure of W phase. The tests indicated that the hardness and wear resistance of the nanostructured W–Cu based composites were greatly improved compared with those of the coarse-grained counterparts[32, 33]. However, due to the increased energy associated with high volume fraction of grain boundaries, the W grains tend to grow rapidly at high temperatures[34–38], leading to loss of some excellent properties derived from the nanostructure[39,40]. Therefore, to keep a high thermal stability of the nanostructure in the W–Cu composites at elevated temperatures is challenging, and is crucial to achieve the outstanding comprehensive properties of the composites.

In the present work, using the prepared W–Cu based bulk composite with the hierarchical nanostructure, we investigate its thermal stability over a wide temperature

range. Then the mechanical behavior of the nanocrystalline W–Cu based composite will be characterized at both room and high temperatures. Based on the examinations, the mechanisms for the stabilization of the nanostructure in the multicomponent W–Cu based composite, as well as the effect of stability on the high- temperature mechanical properties, will be discussed.

2. Experimental

W–Cu and W–Cu–Cr–ZrC composite bulk materials were prepared by the method of powder metallurgy. The Cu content was designed as 20 wt% for both composites, and the additions of Cr and ZrC were 4 wt% and 1 wt% respectively for the W–Cu–Cr–ZrC composite. A route consisting of two-step ball milling procedures and subsequent SPS densification was used for fabrication of the above composites, the details of which were described in our previous work[41].

The thermal stability of the composite samples was investigated by heat-treatment in a temperature range from room temperature to 1000°C. The heat-treated samples were quenched from the designed temperatures to observe the corresponding microstructures and measure the grain sizes. The compressive stress-strain behavior at different temperatures was tested in a range from room temperature to below 1000°C, which was performed on a thermal cycle simulation testing machine. For the compression tests, the composite bulk materials were firstly machined into cylindrical shape with dimensions of Φ6 mm × 9mm, and then welded to thermo-couple for measuring the real-time

temperature of the sample. In the compression process, the samples were heated with a rate of 10℃/s, and then compressed with a strain rate of $0.02s^{-1}$ at each designed temperatures.

The scanning electron microscopy (SEM) and transmission electron microscopy (TEM) were used to observe microstructures of the samples. The energy dispersive spectroscopy (EDS) maps were acquired via high- angle annular dark-field (HAADF) imaging in an aberration-corrected scanning transmission electron microscope (STEM). The grain size was determined by the line intercept method. The hardness was measured by the Vickers hardness tester with a load of 30 kg. Atom probe tomography (APT) characterizations were performed in a local electrode atom probe LEAP 5000 XR. The samples were analyzed at 60 K in laser mode, at a pulse repetition rate of 125kHz, a pulse energy of 30 pJ, and an evap- oration detection rate of 0.2% atom per pulse.

3. Results and discussion

3.1 Microstructures of the prepared composite bulks

Fig. 1 shows the microstructures of the W phase in the prepared W–Cu and W–Cu–Cr–ZrC composite bulk samples. As measured, the mean grain size of W phase in the W–Cu composite is $< d > = 120$ nm (Fig. 1a), while the mean grain size of W phase in the W–Cu–Cr–ZrC composite is much smaller with a value of <d>=39nm (Fig. 1b). It indicates that the grain size of W phase is remarkably decreased to a third of that in the binary W–Cu composite due to the addition of Cr and ZrC. From comparison between these two kinds

of composites, it is expected that the co-addition of Cr and ZrC has important effect on retaining the nanostructure in the W–Cu based composite.

The existing forms and distributions of Cr and ZrC in the micro- structure of the W–Cu–Cr–ZrC composite were examined, and the typical micrographs and composition analysis results are shown in Figs. 2–4. It is observed from Fig. 2a that the grain boundaries of the W phase are strongly pinned by the ultrafine nanoparticles. Particularly, these nanoparticles mainly distribute at the grain triple junctions in the W phase. The composition analyses shown in Fig. 2(b–d) indicate that besides the element Zr the nanoparticles also contain a slight content of Cr, suggesting these nanoparticles are Zr–Cr–C precipitates. The formation of Zr–Cr–C precipitates is further confirmed by the fast Fourier transformation (FFT) from the high-resolution image of the nanoparticle, as shown in Fig. 2(e and f). The precipitates have the same crystal structure with ZrC, but with a smaller interplanar space. The reduced interplanar space is considered to be caused by the substitution of Zr sites by Cr atoms. Furthermore, the Zr–Cr–C nanoparticles tend to form coherent interface with the W matrix, which is beneficial to improve the interfacial thermal stability and the bonding strength[42]. Moreover, Cr mainly distributes along the W grain boundaries in a form of thin film (Fig. 2c), implying that segregation of Cr atoms from the state of W(Cr) solid solution in the synthesized initial powder, i.e. phase separation, occurred. On the other side, in the sintering procedure of the initial powder mixture of W(Cr), ZrC and Cu, the Zr–Cr–C particles formed during the dissolution-precipitation processes. Both the Cr films generated from phase separation and the precipitated Zr–Cr–C nanoparticles inhibit the grain growth of W phase

effectively, which result in a fine nanograin structure of the W phase in the composite.

The composition analysis of the W grain interior is shown in Fig. 3. Corresponding to the region highlighted by the rectangle in a W grain (Fig. 3a), clusters with dark contrast are observed in the lattice structure of the W crystal (Fig. 3b). The EDS analysis (Fig. 3c) indicates they are Cr-enriched clusters in the W crystal. It revealed that Cr atoms dissolved into W lattice and formed clusters having coherent relationship with the W matrix. The APT characterizations of a W grain are given in Fig. 3 (d–g). A cluster visualized by the 20 at.% Cr concentration isosurfaces was observed. 1-nm-thick atom maps through the center of the cluster are shown in Fig. 3e and f, in which the relative positions and extents of the W (red) and Cr (blue) atoms are indicated. The proximity histogram based on the 20 at.% Cr concentration isosufrace shows an obvious enrichment of Cr in the cluster, which is in consistent with the TEM/EDS results.

The Cu grain structure and the corresponding composition analysis are shown in Fig. 4. As shown by the high-resolution TEM image in Fig. 4b, the Cu phase has even smaller grain size than that of W phase. The W/Cu interface with disordered atomic arrangement is observed. It is generally considered that the bonding strength of this kind of interface is weak due to the intrinsic immiscible feature of the different components[43]. The APT characterization of a Cu grain interior (Fig. 4c–f) indicates that W and Cr dissolved in the Cu crystal, with concentrations of 0.83 at.% and 0.06 at.% respectively in the sampled area. As reported in the literature[11,41,44], the substitutional solid solution of metal atoms in the Cu crystal structure will inhibit grain growth and facilitate to form the nanograin structure of Cu phase. Moreover, a higher con- centration of W solid solution

in the Cu grain interior may result in a significant enhancing effect on the strength of the composite.

From the results in Figs. 2–4, the ultrafine nanograin structures in both W and Cu phases, the Cr solid-solution strengthening of W and Cu grains, and additionally W solid-solution strengthening of Cu grains, will result in an increased hardness and strength in the W–Cu–Cr–ZrC composite compared to the conventional binary W–Cu composite. This is verified by the tests of the corresponding samples at the as-prepared state. The hardness and compressive strength of the W–Cu–Cr–ZrC composite are 943 HV and 1799 MPa, respectively, which are 1.2 and 2.1 times as large as those of the W–Cu composite (770 HV and 860 MPa). To study the changes of microstructure and mechanical perfor- mance of the W–Cu–Cr–ZrC composite with temperature, in the following section the thermal stability of the nanostructure in the composite will be examined at a series of temperatures, and the mechanical properties will be tested correspondingly.

3.2 Thermal stability of the nanostructured W–Cu–Cr–ZrC composite

The nanocrystalline W–Cu–Cr–ZrC composite was heat-treated in a temperature range from 400 to 1000°C, at each designed temperature a holding time of 2h was applied. Fig. 5 shows the typical microstructures and the measured grain size distributions of the W phase in the com- posite at the heat-treated temperatures of 400, 600 and 800°C, respectively. It is seen that the nanostructure in the W phase exhibits good thermal

stability with the increase of temperature. Particularly, the mean grain size of W phase has very little change compared to the initial grain size of W phase in the as-prepared W–Cu–Cr–ZrC composite. The selected-area diffraction patterns (SADP) and their indexing (Fig. 5b, e, and h) confirmed the very fine nanograin structure in the W phase.

The changes of the mean grain size of W phase with the heat- treatment temperature are shown in Fig. 6, where the thermal stability of the grain structure is compared between the W–Cu and W–Cu–Cr–ZrC composites. In a wide range from room temperature to 1000°C, the mean grain size of W phase in the W–Cu composite increased by 30%. In contrast, in the same temperature range, the mean grain size of W phase in the W–Cu–Cr–ZrC composite kept almost unchanged. The grain size in the sample after heat-treatment at 1000 °C is nearly the same as the initial grain size of the composite. The even smaller grain size at 1000°C than at lower temperatures is attributed to the phase separation of Cr in the W phase, which can refine the grain structure during the heat-treatment[45]. To further test the thermal stability of the nanostructured W–Cu–Cr–ZrC composite, heat-treatment at elevated temperature up to 1100°C was carried out, which was also made for the W–Cu counterpart for comparison. As is known, this heating temperature is higher than the melting point of Cu (1083°C), thus during the heat-treatment of the binary W–Cu composite, the melted Cu flowed towards the surface of the bulk sample. Consequently, a "golden" surface was formed covering the W–Cu composite sample, as shown in the inset of Fig. 6. However, for the nanostructured W–Cu–Cr–ZrC composite sample, during the heat-treatment at 1100°C, there was no melted Cu present on the surface of the sample. This can be explained by the alloying effect of Cr.

The addition of Cr can reduce the wetting angle between W and Cu, and improve the interfacial bonding strength[46,47]. The above results indicate distinctly that the nano-structured W–Cu–Cr–ZrC composite has much higher thermal stability than the W–Cu composite.

To demonstrate the effects of additions of Cr and ZrC on the for- mation and stabilization of the nanostructure in the W–Cu based composite, a schematic diagram is shown in Fig. 7. For the initial powder mixture, after high-energy ball milling, Cr dissolved in W and the su- persaturated solid solution was formed. The refined ZrC particlesdispersed between the W(Cr) particles. These ZrC particles can provide the nucleation sites during the process of phase separation of W(Cr), leading to a relatively homogeneous distribution of Cr films along W grain boundaries. During sintering of the initial composite powder, the Zr–Cr–C ternary phase formed in the dissolution-precipitation processes, where the reaction between Cr and ZrC was also involved. The resultant Zr–Cr–C phase distributed at W grain boundaries in a form of very fine nanoparticles, which existed particularly at the triple junctions of W grains. Therefore, with the preparation route consisting of high-energy ball milling and SPS sintering procedures, the separated Cr and in-situ precipitated Zr–Cr–C particles, which exist along the grain boundaries and at the grain triple junctions respectively, inhibit effectively migration of grain boundaries in both processes of preparation and heattreatment of the composite material. As a result, the nanostructured composite has a high thermal stability at high temperatures even up to the melting point of Cu.

In order to make clear whether the thermal stability of the nanostructure of W phase

depends on the holding time at the high temperature, a further step of heat-treatment was performed for the W–Cu–Cr–ZrC composite, in which the samples were held at 1000°C for different times. The microstructures and measured grain sizes at different stages are shown in Fig. 8. It can be seen that after heat-treatment at 1000°C for 12h, the mean grain size of W phase increased to about 92nm (Fig.8g). This implies that when being kept at high temperatures for a long time, obvious grain growth may occur in the W phase. Nevertheless, the mean grain size of W phase still remained at the nanoscale after such a long duration at a high temperature close to Cu melting point.

As observed in Fig. 8c, with the increase of heat-treatment duration, the number of particles decreases and the size of particles increases (as indicated by the arrows). To detect the composition of the particles, EDS analysis was firstly performed for the W phase in the W–Cu–Cr–ZrC sample heat-treated at 1000°C for 12 h. The results in Fig. 8(d–f) indicate that the particles with larger size and darker contrast are Cr-rich phase. To determine the particle composition, APT characterizations were performed for the local W phase containing part of W grain and a neighboring particle, as shown in Fig.9. The partition of W to the upper part and Cr and C to the lower part are clearly evident. The atomic ratio of (Cr+W):C in the lower part is approximately 23:6, suggesting that these Cr-enriched carbides are of $Cr_{23}C_6$-type with certain amounts of W substitutional for partial Cr. This kind of bimetallic carbide can keep the original cubic crystal structure[48]. Moreover, the W phase is not pure W but contains approximately 5 at.% Cr (Fig. 9b, f). Thus, it can be inferred that the growth of W grains at high temperatures is closely related with the diffusion of phase separation element Cr. In this process, it tends to form larger

$(Cr,W)_{23}C_6$ particles between W grains (Fig. 8c, e) from distributing at W grain boundaries in a form of thin film (Fig. 2). As a result, the inhibiting effect on the grain coarsening is weakened.

The distribution state of Zr in the W phase, as shown in Fig. 8f, indicates that Zr diffused from the Zr–Cr–C nanoparticles distributing at the triple junctions of W grains to the grain interiors during isothermal holding at 1000°C for 12h. This implies that the strong pinning effect of Zr–Cr–C precipitates on the migration of W grain boundaries vanished. Therefore, during the long-term heat-treatment, due to the atomic diffusion and the resultant evolution of Cr and Zr distributions in the W phase, the obvious grain growth occurred. It can be concluded that the thermal stability of the nanograin structure is strongly influenced by the diffusion and segregation of Cr towards $(Cr,W)_{23}C_6$ particles between W grains and the tendency of Zr random distribution in the W phase.

3.3 Mechanical performance at high temperatures

From the characterizations in Section 3.2, it revealed that the nanostructure in the W–Cu–Cr–ZrC composite has good thermal stability at high temperatures and the grain size of W phase can be kept at the nanoscale up to 1000°C, even after heat-treatment for a long duration. In this section, the mechanical behavior of the W–Cu based composites at high temperatures will be investigated.

The high-temperature compression tests were carried out for the W–Cu and W–Cu–Cr–ZrC samples to examine the effects of grain structure and its thermal stability on the fracture strength of the composite. The compressive strength at different testing

temperatures are shown in Fig. 10a for the two kinds of composites. At the room temperature, both W–Cu and W–Cu–Cr–ZrC composites exhibit the highest compressive strength compared with those at the increased temperatures, which is due to the higher Pinar force at the lower temperature that results in a sharp increase in the yield strength[39]. The room-temperature compressive strength of the nanostructured W–Cu–Cr–ZrC composite is about twice that of the W–Cu composite. In addition, the compressive strength of the W–Cu composite decreased significantly with the increase of temperature, while the strength of the nanostructured composite almost had no change when the temperature was increased from 300℃ to 700℃. With the temperature further increased to 900℃, the strength of the nanostructured W–Cu–Cr–ZrC composite decreased to 1150MPa, which is still approximately four times as high as that of the W–Cu composite (about 300MPa). Although with lower content of Cu the strength of W–Cu composites can be increased, the strength of the present nanostructured W–Cu–Cr–ZrC with 20 wt% Cu at 900℃ is more than three times as high as that of the coarse-grained W–Cu with 10 wt% Cu (about 350 MPa) reported in the literature for the same testing temperature[50].

It is worthy to note that in addition to the grain size, the deformation temperature plays a significant role in the strength of the composite. In our previous work, it was found that with the increase of temperature, the dislocations are more likely to nucleate and slip due to the reduced critical resolved shear stress on the slip planes[49], which results in a decrease in the strength of the material at high temperatures. In the present work, the nanostructure of the W phase in the W–Cu–Cr–ZrC composite has a high thermal

stability with the increase of the temperature, this assures a high strength of the composite at high tem- peratures from the aspect of grain size. However, the increase in the density of movable dislocations at high temperatures leads to the decrease in the strength of the composite despite the little change in the grain size.

Fig. 10b shows the measured results of the hardness of the W–Cu and W–Cu–Cr–ZrC composite samples heat-treated at 1000°C for different times, together with those of the as-prepared composite materials for comparison. It can be seen that after heat-treatment at 1000°C for 2 h, the hardness of the W–Cu–Cr–ZrC composite had a decrease of only about 3%, while that of the W–Cu composite decreased by 12%. This change in the hardness is consistent with the microstructure evolution during the heat-treatment, i.e. the change of the grain size, as shown in

Fig. 8g. When the heat-treatment duration is further extended to 12h, the W–Cu–Cr–ZrC composite still had an excellent hardness of 770 ± 24HV, which is much higher than that of the W–Cu composite under the same condition, and is nearly the same as the hardness of the W–Cu composite at the room temperature. The measurements of the hardness and strength at high temperatures indicate distinctly the importance of the nanostructure and its thermal stability to the mechanical performance of W–Cu based composites.

From the above experimental results regarding the microstructure and mechanical properties as a function of temperature, it is found that the nanostructured W–Cu–Cr–ZrC composite has higher hardness and strength at high temperatures than the binary W–Cu

composite prepared by the same Cu powder and the sintering process. The excellent properties are attributed to the stable nanostructure within the W phase of the composite, which is achieved by the phase separation element and the dispersive in-situ precipitated nanoparticles. As the temperature is below 900°C, the nanostructure is stabilized through inhibiting migration of grain boundaries by the separated Cr thin films and Zr–Cr–C nanoparticles precipitated at the grain triple junctions. When the temperature is further increased, the Cu phase is softened and the plastic deformation becomes larger under the compressive load. Due to the nanostructure in the W phase of the W–Cu–Cr–ZrC composite, dislocations can hardly form or move because of the hindering of plenty of grain boundaries in the W phase. This results in a much higher strength of the nanostructured composite than that of the binary coarse-grained counterpart.

For the W–Cu based composites, the trade-off between the strength and plasticity exists, as similar as that in the metallic materials. However, in contrast to the metals and alloys that have single phases hence limitation in the plastic accommodation between the hard and soft phases, the W–Cu based composites are flexible to adjust the plasticity by tailoring the content of Cu phase. Thus, excellent comprehensive mechanical properties can be achieved in the nanostructured W–Cu based composites, based on establishment of the cooperation between the Cu content and appropriate grain size of W phase. This will be a future research direction of our work, and the present study is focused on the temperature dependence of the strength and the effect of the thermal stability of the microstructure of the composites.

4. Conclusions

The microstructure evolution and mechanical behavior at different temperatures have been investigated for the prepared nanostructured W–Cu–Cr–ZrC composite, together with those of the binary coarsegrained W–Cu composite for comparison. The thermal stability of the nanostructure in the composite was characterized, and its mechanisms and effect on the mechanical properties at high temperatures were disclosed . The main conclusions are drawn.

(1) Nanostructured W–Cu based composite bulk was prepared by sintering the powders with co-addition of phase separation element Cr and ZrC particles. The ZrC nanoparticles highly dispersed in the W phase play an important role in promotion of re-distribution of Cr thin films along grain boundaries and precipitation of Zr–Cr–C nanoparticles at grain triple junctions, which result in a homogeneous grain structure of W phase with a mean grain size that is as small as 39nm.

(2) The mean grain size of W phase in the nanostructured W–Cu–Cr–ZrC composite had little change in a wide range from room temperature up to 1000℃ at a duration of 2 h, exhibiting an outstanding thermal stability of the nanostructure at high temperatures. It is attributed to the separated Cr films and in-situ precipitated Zr–Cr–C nanoparticles which inhibit strongly migration of grain boundaries during the heat-treatment. When extending isothermal holding to a long duration, diffusion segregation of Cr and random re-distribution of Zr occurred, leading to grain growth of W phase.

(3) The nanostructured W–Cu–Cr–ZrC composite showed remarkably enhanced

hardness and strength compared with the binary coarse-grained W–Cu composite. The compressive strength of the nanostructured composite achieved 1150MPa at 900℃, which is approximately four times as high as that of the coarse-grained counterpart. The excellent high-temperature mechanical prop- erties of the W–Cu–Cr–ZrC composite result from the high ther- mal stability of the nanostructure in the W phase. It demonstrated the crucial role of W skeleton in the overall strength of the composite at both room and high temperatures.

Declaration of competing interest

The authors declare that they have no known competing financial interests or personal relationships that could have appeared to influence the work reported in this paper.

Acknowledgements

This work was supported by the National Natural Science Foundation of China (51631002, 51701007 and 51621003).

References

[1] Hou C, Song XY, Tang FW, Li YR, Cao LJ, Wang J, et al. W–Cu composites with submicron-and nanostructures: progress and challenges. NPG Asia Mater 2019;11: 74–94.

[2] Bregel T, Krauss-Vogt W, Michal R, Saeger KE. On the application of W/Cu materials in the fields of power engineering and plasma technology. IEEE Trans Compon Hybrids Manuf Technol 1991;14:8–13.

[3] Dong LL, Ahangarkani M, Chen WG, Zhang YS. Recent progress in development of tungsten-copper composites: fabrication, modification and applications. Int J Refract Met Hard Mater 2018;75:30–42.

[4] Tejado E, Müller AV, You JH, Pastor JY. Evolution of mechanical performance with temperature of W/Cu and W/CuCrZr composites for fusion heat sink applications. Mater Sci Eng, A 2018;712:738–46.

[5] Mileiko ST, Kolchin AA, Galyshev SN, Shakhlevich OF, Prokopenko VM. Oxide- fibre/molybdenum-alloy-matrix composites: a new way of making and some mechanical properties. Composites Part A 2020;132:105830.

[6] Hou C, Wang J, Wang HB, Liu XM, Liang SH, Song XY, et al. Nanoporous tungsten with tailorable microstructure and high thermal stability. Int J Refract Met Hard Mater 2018;77:128–31.

[7] Lee D, Umer MA, Ryu HJ, Hong SH. Elevated temperature ablation resistance of HfC particle-reinforced tungsten composites. Int J Refract Met Hard Mater 2014; 43:89–93.

[8] Tejado E, Müller A, You JH, Pastor JY. The thermo-mechanical behaviour of W-Cu metal matrix composites for fusion heat sink applications: the influence of the Cu content. J Nucl Mater 2018;498:468–75.

[9] Wang YK, Xie ZM, Wang MM, Deng HW, Yang JF, Jiang Y, et al. The superior thermal stability and tensile properties of hot rolled W-HfC alloys. Int J Refract Met Hard Mater 2019;81:42–8.

[10] Hou QQ, Huang K, Luo LM, Tan XY, Zan X, Xu Q, et al. Microstructure and its high temperature oxidation behavior of W-Cr alloys prepared by spark plasma sintering. Materialia 2019;6:100332.

[11] Zhao JT, Zhang JY, Hou ZQ, Wu K, Feng XB, Liu G, et al. The W alloying effect on thermal stability and hardening of nanostructured Cu–W alloyed thin films. Nanotechnology 2018;29:195705.

[12] Moszner F, Cancellieri C, Chiodi M, Yoon S, Ariosa D, Janczak-Rusch J, et al. Thermal stability of Cu/W nano-multilayers. Acta Mater 2016;107:345–53.

[13] Dong Z, Liu N, Ma ZQ, Liu CX, Guo QY, Liu YC. Preparation of ultra-fine grain W- Y2O3 alloy by an improved wet chemical method and two-step spark plasma sintering. J Alloys Compd 2017;695:2969–73.

[14] Lu ZL, Luo LM, Chen JB, Huang XM, Cheng JG, Wu YC. Fabrication of W–Cu/CeO2 composites with excellent electric conductivity and high strength prepared from copper-coated tungsten and Ceria powders. Mater Sci Eng, A 2015;626:61–6.

[15] Yang XH, Liang SH, Wang XH, Xiao P, Fan ZK. Effect of WC and CeO2 on microstructure and properties of W–Cu electrical contact material. Int J

Refract Met Hard Mater 2010;28:305–11.

[16] Luo LM, Lu ZL, Huang XM, Tan XY, Luo GN, Cheng JG, et al. Fabrication of W–Cu/ La2O3 composite powder with a novel pretreatment prepared by electroless plating and its sintering characterization. Int J Refract Met Hard Mater 2015;48: 1–4.

[17] Zhang CC, Luo GQ, Zhang J, Dai Y, Shen Q, Zhang LM. Synthesis and thermal conductivity improvement of W-Cu composites modified with WC interfacial layer. Mater Des 2017;127:233–42.

[18] Zhang Q, Liang SH, Zhuo LC. Fabrication and properties of the W-30wt% Cu gradient composite with W@WC core-shell structure. J Alloys Compd 2017;708: 796–803.

[19] Dong LL, Huo WT, Ahangarkani M, Zhang B, Zhao YQ, Zhang YS. Microstructural evaluation and mechanical properties of in-situ WC/W-Cu composites fabricated by rGO/W-Cu spark plasma sintering reaction. Mater Des 2018;160:1196–207.

[20] Yang XH, Fan ZK, Liang SH, Xiao P. Effects of TiC on microstructures and properties of CuW electrical contact materials. Rare Met Mater Eng 2007;36: 817–21.

[21] Heuer S, Lienig T, Mohr A, Weber T, Pintsuk G, Coenen J, et al. Ultra-fast sintered functionally graded Fe/W composites for the first wall of future fusion reactors. Composites Part B 2019;164:205–14.

[22] Zhuo LC, Zhao Z, Qin ZC, Chen QY, Liang SH, Yang X, et al. Enhanced mechanical and arc erosion resistant properties by homogenously precipitated nanocrystalline fcc-Nb in the hierarchical W-Nb-Cu composite. Composites Part B 2019;161:336–43.

[23] Tang XQ, Zhang HB, Du DM, Qu D, Hu CF, Xie RJ, et al. Fabrication of W–Cu functionally graded material by spark plasma sintering method. Int J Refract Met Hard Mater 2014;42:193–9.

[24] Liu R, Hao T, Wang K, Zhang T, Wang XP, Liu CS, et al. Microwave sintering of W/ Cu functionally graded materials. J Nucl Mater 2012;431:196–201.

[25] Zhao P, Guo SB, Liu GH, Chen YX, Li JT. Fabrication of W–Cu functionally graded material with improved mechanical strength. J Alloys Compd 2014;601:289–92.

[26] Liang CP, Fan JL, Gong HR. Cohesion strength and atomic structure of W-Cu graded interfaces. Fusion Eng Des 2017;117:20–3.

[27] Wan L, Cheng JG, Fan YM, Liu Y, Zheng ZJ. Preparation and properties of superfine W–20Cu powders by a novel chemical method. Mater Des 2013;51:136–40.

[28] Qiu WT, Pang Y, Xiao Z, Li Z. Preparation of W-Cu alloy with high density and ultrafine grains by mechanical alloying and high pressure sintering. Int J Refract Met Hard Mater 2016;61:91–7.

[29] Li BQ, Sun ZQ, Hou GL, Hu P, Yuan FL. Fabrication of fine-grained W-Cu composites with high hardness. J Alloys Compd 2018;766:204–14.

[30] Daoush WM, Yao J, Shamma M, Morsi K. Ultra-rapid processing of high-hardness tungsten–copper nanocomposites. Scripta Mater 2016;113:246–9.

[31] Li YR, Hou C, Lu H, Liang SH, Song XY. WC strengthened W–Cu nanocomposite powder synthesized by in-situ reactions. Int J Refract Met Hard Mater 2019;79: 154–7.

[32] 32.. Hou C, Cao LJ, Li YR, Tang FW, Song XY. Hierarchical nanostructured W-Cu composite with outstanding hardness and wear resistance. Nanotechnology 2019; 31:084003.

[33] Wu WZ, Hou C, Cao LJ, Liu XM, Wang HB, Lu H, et al. High hardness and wear resistance of W-Cu composites achieved by elemental dissolution and interpenetrating nanostructure. Nanotechnology 2020;31:135704.

[34] Deng SH, Yuan TC, Li RD, Zeng FH, Liu GH, Zhou X. Spark plasma sintering of pure tungsten powder: densification kinetics and grain growth. Powder Technol 2017; 310:264–71.

[35] Tang FW, Liu XM, Wang HB, Hou C, Lu H, Nie ZR, et al. Solute segregation and thermal stability of nanocrystalline solid solution systems. Nanoscale 2019;11: 1813–26.

[36] Feltham P. Grain growth in metals. Acta Metall 1957;5:97–105.

[37] Louat N. On the theory of normal grain growth. Acta Metall 1974;22:721–4.

[38] Chookajorn T, Murdoch HA, Schuh CA. Design of stable nanocrystalline alloys. Science 2012;337:951–4.

[39] Meyers MA, Mishra A, Benson DJ. Mechanical properties of nanocrystalline materials. Prog Mater Sci 2006;51:427–556.

[40] Liu G, Zhang GJ, Jiang F, Ding XD, Sun YJ, Sun J, et al. Nanostructured

high-strength molybdenum alloys with unprecedented tensile ductility. Nat Mater 2013; 12:344–50.

[41] Cao LJ, Hou C, Li YR, Liu XM, Liang SH, Song XY. Novel nanocrystalline W–Cu–Cr–ZrC composite with ultra-high hardness. Nanotechnology 2020;31: 134002.

[42] Xie ZM, Liu R, Miao S, Yang XD, Zhang T, Wang XP, et al. Extraordinary high ductility/strength of the interface designed bulk W-ZrC alloy plate at relatively low temperature. Sci Rep 2015;5:16014.

[43] Jiang DF, Long JY, Han JP, Cai MY, Lin Y, Fan PX, et al. Comprehensive enhancement of the mechanical and thermo-mechanical properties of W/Cu joints via femtosecond laser fabricated micro/nano interface structures. Mater Sci Eng, A 2017;696:429–36.

[44] Chakraborty S, Gupta AK, Roy D, Basumallick A. Studies on nano-metal dispersed Cu-Cr matrix composite. Mater Lett 2019;257:126739.

[45] Vilemova M, Illkova K, Lukac F, Matejicek J, Klecka J, Leitner J. Microstructure and phase stability of W-Cr alloy prepared by spark plasma sintering. Fusion Eng Des 2018;127:173–8.

[46] Zou JT, Yang XH, Liu GF, Liang SH. Deformability of Cu-W composites with addition of Cr, Ti activated elements. J Comput Theor Nanosci 2011;4:1017–21.

[47] Li DS, Fan ZK. Effects of chromium and electrical field on wettability between copper and tungsten. Rare Met Mater Eng 2007;36:1008–11.

[48] Lv ZQ, Dong F, Zhou ZA, Jin GF, Sun SH, Fu WT. Structural properties, phase stability and theoretical hardness of Cr23-xMxC6 (M Mo, W; x 0–3). J Alloys Compd 2014;607:207–14.

[49] Hu HX, Liu XM, Hou C, Wang HB, Tang FW, Song XY. How hard metal becomes soft: crystallographic analysis on the mechanical behavior of ultra-coarse cemented carbide. Acta Crystallogr B: Struct Sci Cryst Eng Mater 2019;75:1014–23.

[50] Lin DG, Han JS, Kwon YS, Ha S, Bollina R, Park SJ. High-temperature compression behavior of W–10 wt.% Cu composite. Int J Refract Met Hard Mater 2015;53: 87–91.

Figure captions

Fig. 1. Microstructures of W phase in (a) W–Cu and (b) W–Cu–Cr–ZrC composite bulk samples prepared by the same fabrication process.

Fig. 2. Analysis of composition and crystal structure of the precipitates located at the triple junctions of W grains in the W–Cu–Cr–ZrC composite: (a) HAADF image of W grain structure; (b–d) Elemental distributions of Zr, Cr, and W in the region highlighted by the rectangle in (a); (e, f) Characterizations of the crystal structure of the precipitate and its interface with the W grain.

Fig. 3. Composition analysis of W grain interior of the as-prepared W–Cu–Cr–ZrC composite: (a) HAADF image of W grain structure; (b) High-resolution image corresponding to the W grain interior highlighted by the rectangle in (a), showing W lattice structure containing dark clusters; (c) EDS analysis of the area marked by the cross in (b); (d) 3D atom maps of W and Cr, together with a Cr-enriched cluster. The isosurfaces with a concentration of 20 at.% Cr were used to visualize Cr-enriched cluster; (e, f) High-resolution atom maps showing the atomic distributions of the Cr-enriched cluster; (g) Proximity histogram across the interface between the matrix and cluster.

Fig. 4. Grain structure of Cu phase and composition analysis of the Cu grain: (a) Microstructure of local configuration of W and Cu phases; (b) High-resolution TEM image of Cu grains and W/Cu phase boundary, corresponding to the region highlighted by the rectangle in (a); (c–f) APT characterization of a Cu grain interior, with 3D atom maps of Cu, W, and Cr.

Fig. 5. Microstructures and grain size distributions of W phase in the W–Cu–Cr–ZrC samples heat-treated at different temperatures: (a–c) 400℃; (d–f) 600℃; (g–i) 800℃. (b), (e), and (h) are SADPs and the indexing of W phase at different temperatures. (c), (f), and (i) are the corresponding grain size distributions.

Fig. 6. Changes of grain size of W phase in the W–Cu and W–Cu–Cr–ZrC composites with the heat-treatment temperatures at a holding time of 2h.

Fig. 7. Schematic diagram of the preparation route and microstructural characteristics of the nanostructured W–Cu–Cr–ZrC composite.

Fig. 8. W grain structures of W–Cu–Cr–ZrC samples at different treatment stages: (a) As-prepared; (b) Holding at 1000℃ for 2 h; (c) Holding at 1000℃ for 12h; (d–f) Elemental distributions in the W phase, corresponding to (c); (g) Change of mean grain size of W phase with holding time at 1000℃.

Fig. 9. Composition analysis of the coarse particles in the W–Cu–Cr–ZrC sample heat-treated at 1000℃ for 12h: (a) Microstructure of W grains and coarsened particles; (b–e) 3D atom maps of W, Cr, and C. The isosurfaces with a concentration of 40 at.% Cr were used to visualize Cr-enriched particles; (f) Proximity histogram across the interface between the W grain and particle.

Fig. 10. Comparison of mechanical performance between W–Cu and W–Cu–Cr–ZrC composites: (a) Compressive strength at different temperatures; (b) Hardness at room temperature and after heat-treatment at 1000℃ for different times.

Fig 1

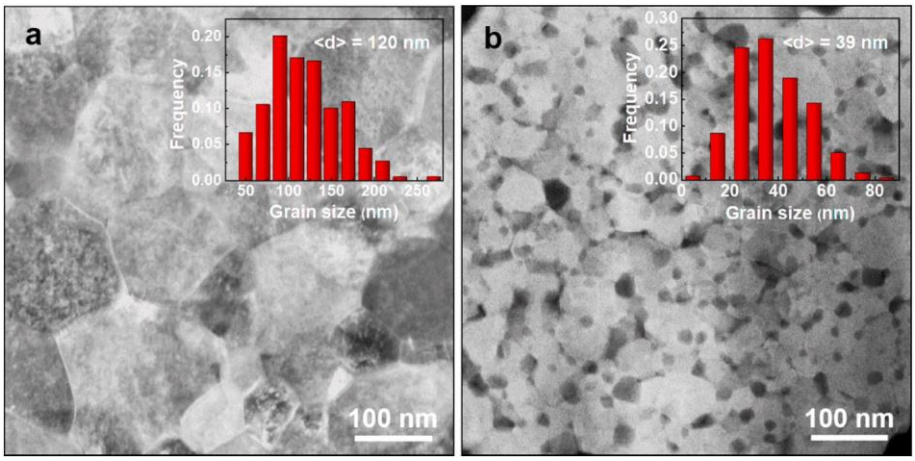
a
<d> = 120 nm
Frequency
0.20
0.15
0.10
0.05
0.00
50
100
150
200
250
Grain size (nm)
100 nm
b
<d> = 39 nm
Frequency
0.30
0.25
0.20
0.15
0.10
0.05
0.00
0
20
40
60
80
Grain size (nm)
100 nm

Fig 2

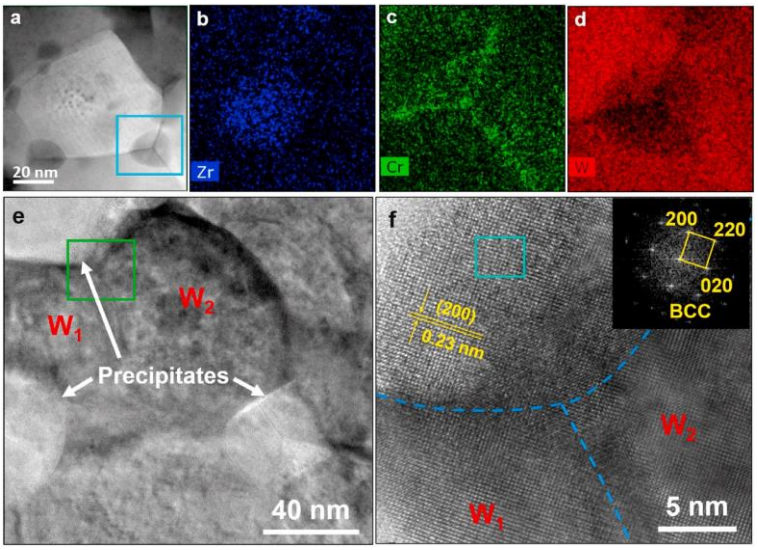
a
20 nm
b
Zr
c
Cr
d
W
e
W1
W2
Precipitates
40 nm
f
200
220
020
BCC
(200)
0.23 nm
W2
W1
5 nm

Fig 3

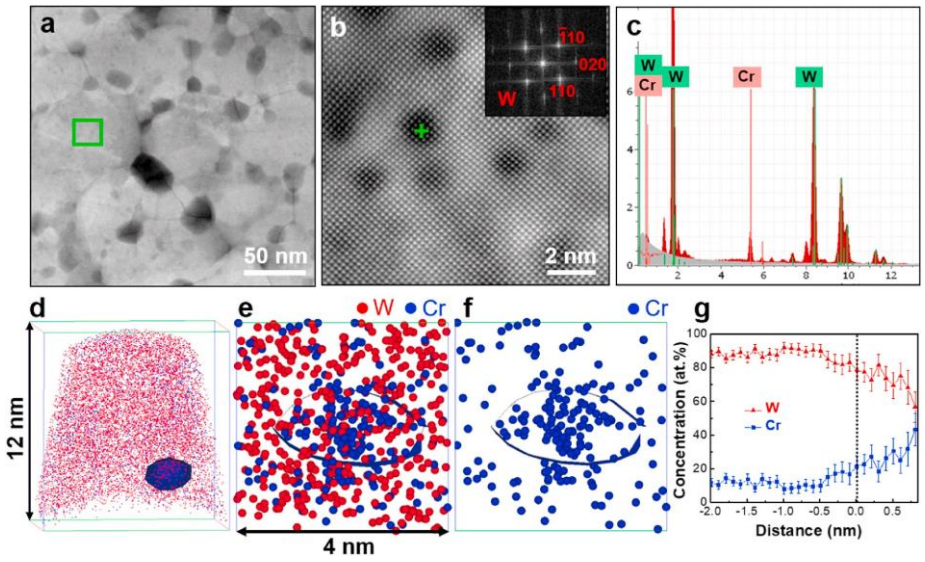
a
50 nm
b
2 nm
$\bar{1}10$
020
W
110
c
W
Cr
W
Cr
W
d
12 nm
e
W Cr
4 nm
f
Cr
g
Concentration (at.%)
W
Cr
Distance (nm)

Fig 4

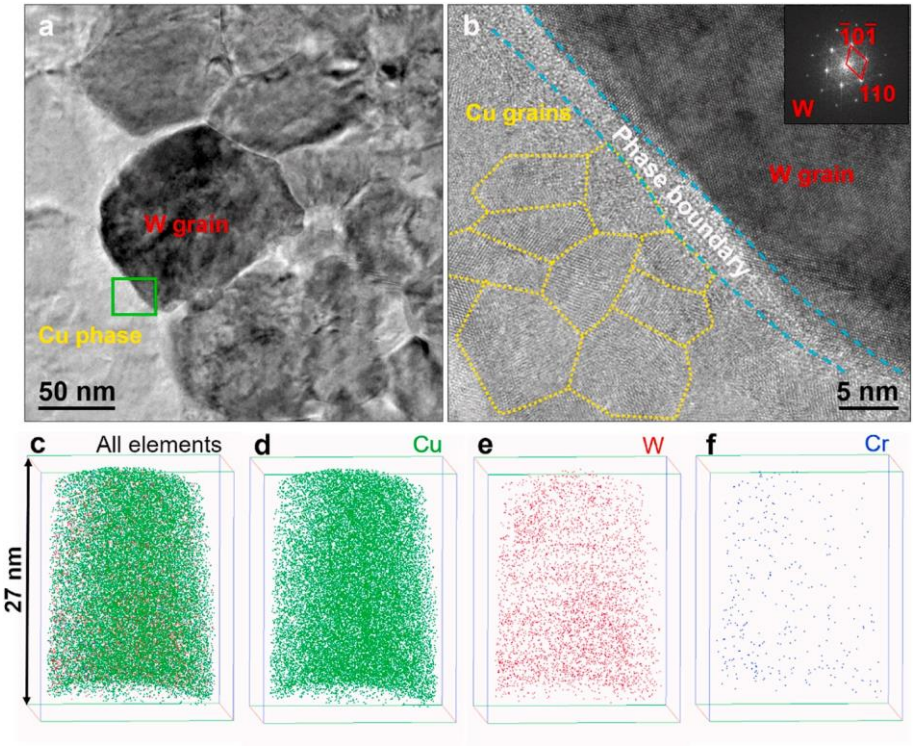
a
W grain
Cu phase
50 nm
b
Cu grains
Phase boundary
W grain
W
5 nm
c All elements
d Cu
e W
f Cr
27 nm

Fig 5

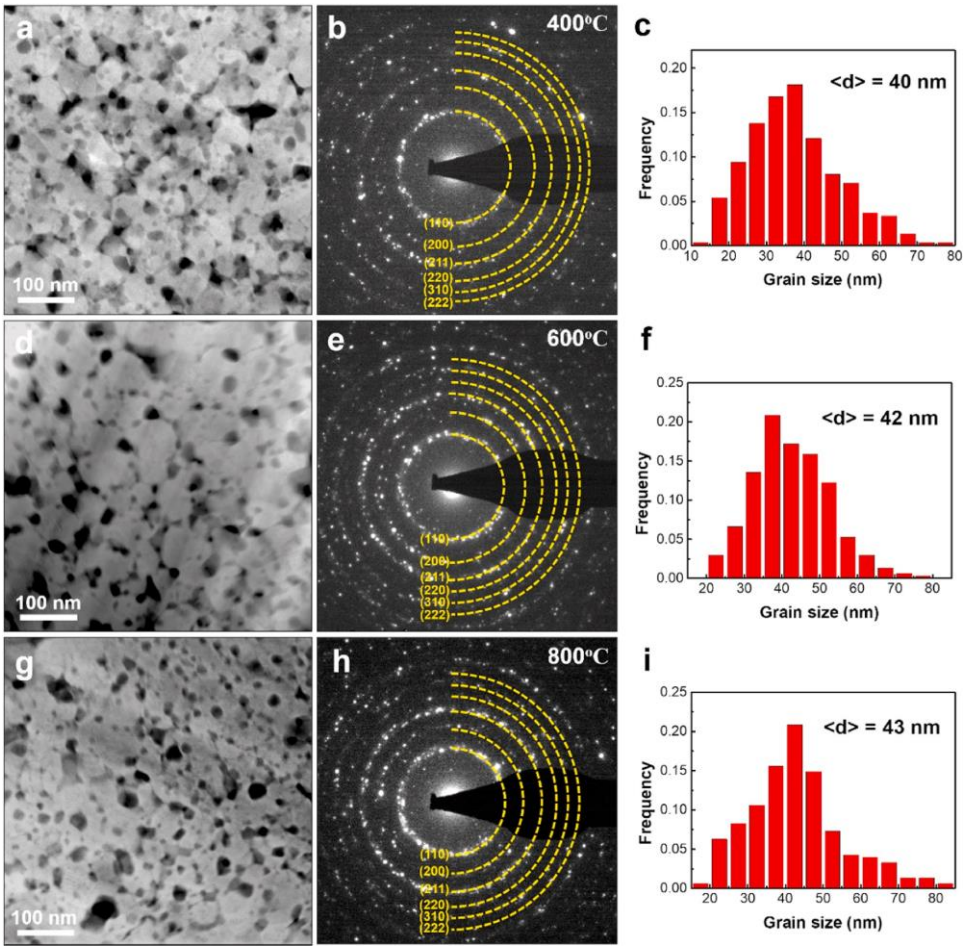
a
b
400°C
c
100 nm
(110)
(200)
(211)
(220)
(310)
(222)
<d> = 40 nm
Frequency
Grain size (nm)
d
e
600°C
f
100 nm
(110)
(200)
(211)
(220)
(310)
(222)
<d> = 42 nm
Frequency
Grain size (nm)
g
h
800°C
i
100 nm
(110)
(200)
(211)
(220)
(310)
(222)
<d> = 43 nm
Frequency
Grain size (nm)

Fig 6

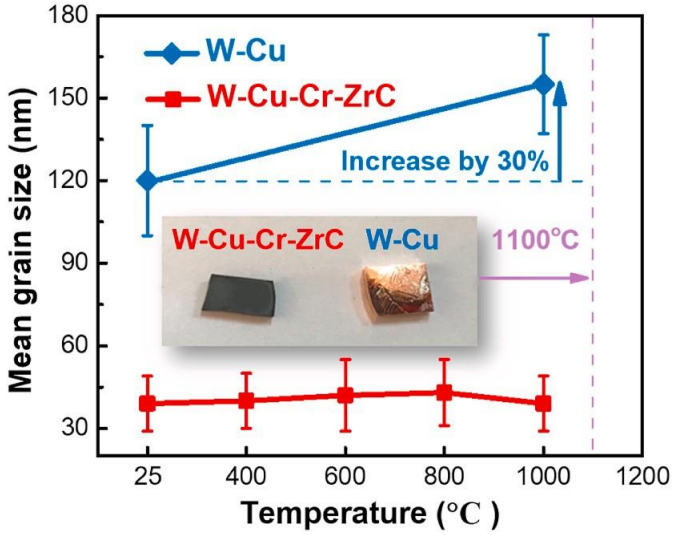
W-Cu
W-Cu-Cr-ZrC
Increase by 30%
W-Cu-Cr-ZrC
W-Cu
1100°C
Mean grain size (nm)
180
150
120
90
60
30
25
400
600
800
1000
1200
Temperature (°C)

Fig 7

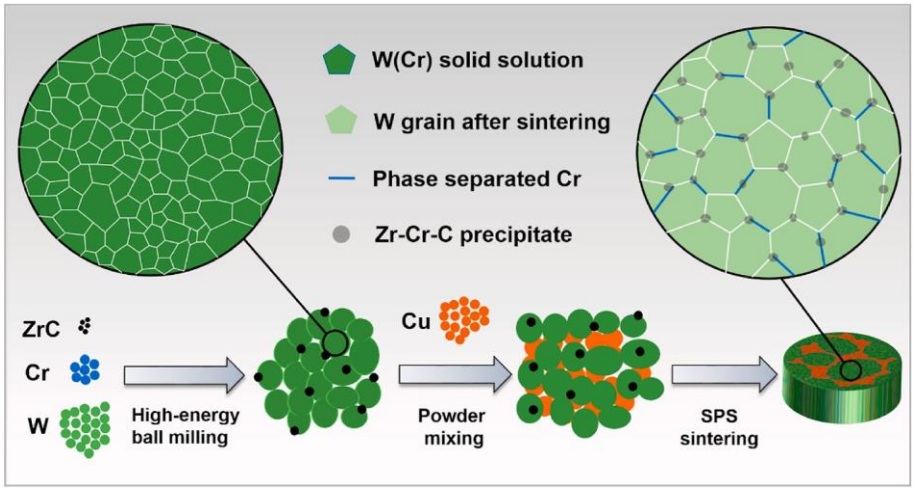
W(Cr) solid solution
W grain after sintering
Phase separated Cr
Zr-Cr-C precipitate
ZrC
Cr
W
High-energy ball milling
Cu
Powder mixing
SPS sintering

Fig 8

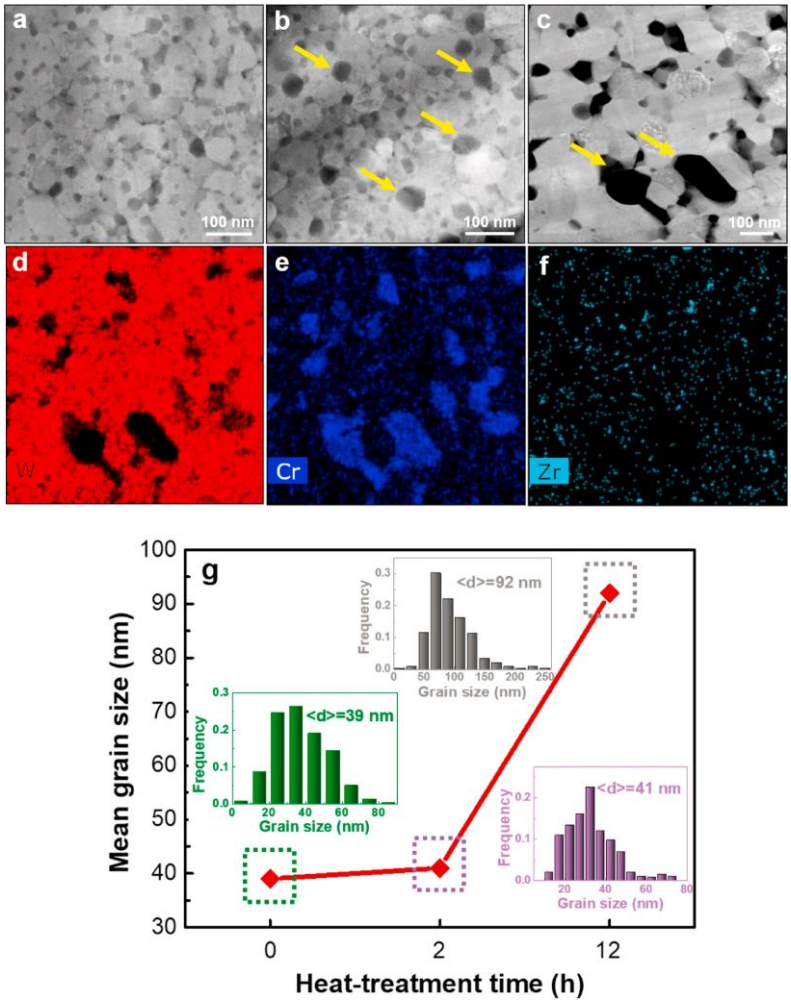
a
b
c
100 nm
100 nm
100 nm
d
e
f
W
Cr
Zr
g
Mean grain size (nm)
Heat-treatment time (h)
<d>=92 nm
<d>=39 nm
<d>=41 nm
Frequency
Grain size (nm)

Fig 9

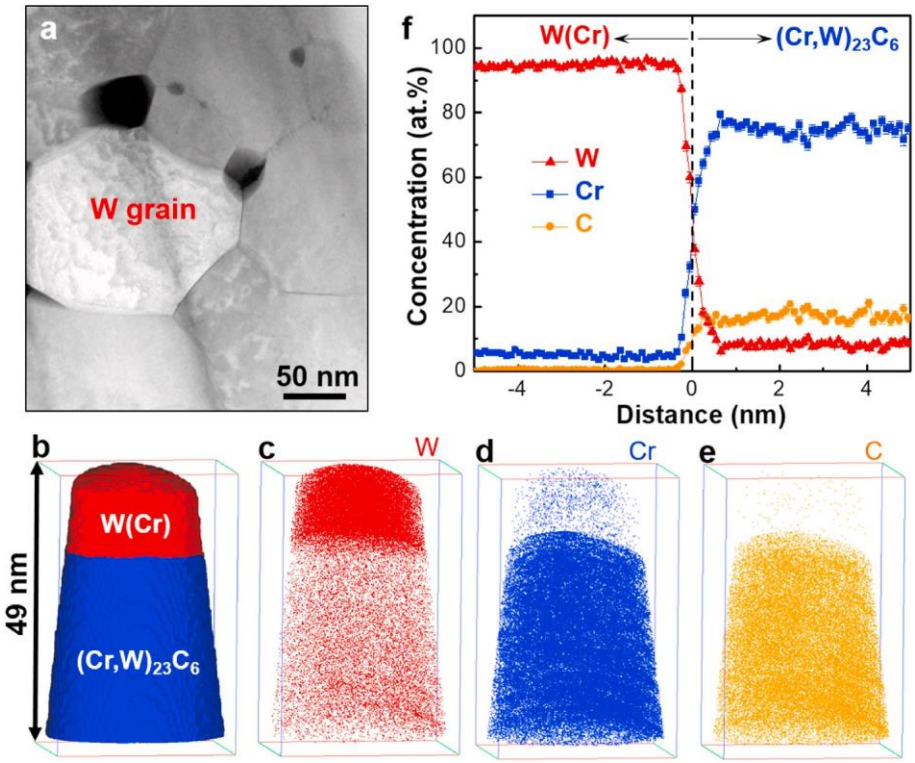
a
W grain
50 nm
f
W(Cr)
(Cr,W)23C6
Concentration (at.%)
W
Cr
C
Distance (nm)
b
W(Cr)
(Cr,W)23C6
49 nm
c
W
d
Cr
e
C

Fig 10

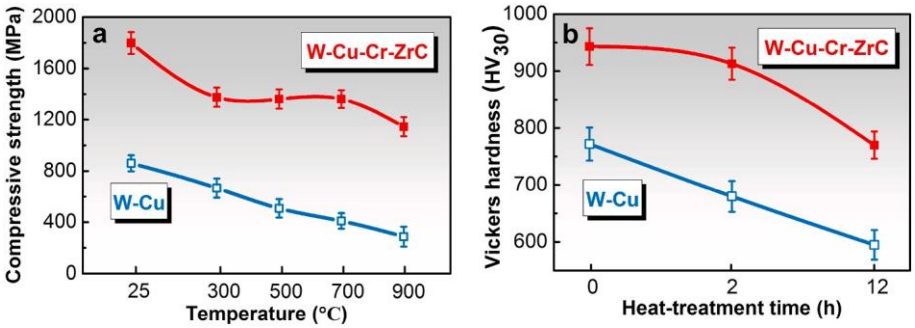
a
W-Cu-Cr-ZrC
W-Cu
Compressive strength (MPa)
2000
1600
1200
800
400
0
25
300
500
700
900
Temperature (°C)
b
W-Cu-Cr-ZrC
W-Cu
Vickers hardness (HV30)
1000
900
800
700
600
0
2
12
Heat-treatment time (h)